

# Magnetic–Plasmonic FePt@Ag Core–Shell Nanoparticles and Their Magnetic and SERS Properties

Nguyen T. T. Trang · Trinh T. Thuy ·  
Koichi Higashimine · Derrick M. Mott ·  
Shinya Maenosono

Received: 27 November 2012 / Accepted: 25 February 2013 / Published online: 9 March 2013  
© Springer Science+Business Media New York 2013

**Abstract** Magnetic–plasmonic FePt@Ag core–shell nanoparticles (NPs) with different Ag shell thicknesses were successfully synthesized using a seed-mediated method. They presented not only localized surface plasmon resonance in the visible region, but also superparamagnetic behavior at room temperature. When normalized by the weight of FePt, the saturation magnetization of the FePt@Ag NPs was found to be higher than that of FePt NPs, suggesting that the Ag shell effectively passivated the FePt NP surfaces, avoiding the direct interaction between the FePt core and surface capping ligands that typically forms a magnetically dead layer in FePt NPs. Despite the high colloidal stability and the small size of the FePt@Ag NPs, the NPs were easily separated using a permanent magnet. The surface enhanced Raman scattering (SERS) activity of the FePt@Ag NPs was then examined using thiophenol as a Raman reporter molecule and was found to be equivalent to that of Ag NPs. Moreover, the SERS activity of the FePt@Ag NPs was enhanced when a magnetic field was applied during the preparation of the SERS substrate (FePt@Ag NP film). These FePt@Ag NPs hold promise as dual-functional sensing probes for environmental and diagnostic applications.

**Electronic supplementary material** The online version of this article (doi:10.1007/s11468-013-9529-7) contains supplementary material, which is available to authorized users.

N. T. T. Trang · T. T. Thuy · K. Higashimine · D. M. Mott ·  
S. Maenosono (✉)  
School of Materials Science, Japan Advanced Institute  
of Science and Technology (JAIST), 1-1 Asahidai,  
Nomi, Ishikawa 923-1292, Japan  
e-mail: shinya@jaist.ac.jp

N. T. T. Trang  
Institute of Materials Science, Vietnam Academy  
of Science and Technology (VAST), 18 Hoang Quoc Viet,  
Hanoi, Vietnam

**Keywords** Iron–platinum nanoparticle · Silver shell ·  
Magnetic separation · Surface enhanced Raman scattering

## Introduction

Currently, nanoparticles (NPs) composed of different materials with multiple functions or properties—e.g., magnetic–plasmonic [1, 2], magnetic–fluorescent [3, 4], or metal–semiconductor [5]—have received much attention, because they exhibit a multifunctionality stemming from the different components that is difficult to reproduce in single-component NPs. Plasmonic (especially Au and Ag) NPs are ideal candidates for various sensing/imaging applications—including chemical/biological sensors, cellular imaging, immunodiagnosis, DNA sequencing, and photothermal therapy—because of their excellent localized surface plasmon resonance (LSPR) and surface enhanced Raman scattering (SERS) properties. Magnetic NPs (especially superparamagnetic NPs) are also promising materials for various applications, including the magnetic separation of chemicals/biomolecules/cells, site-specific drug delivery, magnetic resonance imaging (MRI), magnetic immunodiagnosis, and hyperthermia. The combination of plasmonic and magnetic materials in a single nanostructure has the potential to open up new applications in biology, such as immunomagnetic separation under plasmonic imaging monitoring, dual mode imaging (MRI and plasmonic imaging), and SERS sensing.

There have been a number of reports on the combination of magnetic NPs with plasmonic materials for different purposes. For example, Fe<sub>3</sub>O<sub>4</sub>–Ag heterodimers [6], Fe<sub>3</sub>O<sub>4</sub>@Au core–shell NPs [7], and FePt@Au core–shell NPs [8] have been reported. Among those magnetic–plasmonic NPs, FePt@Ag NPs seem to be better suited for biological sensing/imaging applications when compared

with other magnetic–plasmonic NPs, in terms of their size (less than 20 nm), magnetic properties (especially the saturation magnetization,  $M_s$ ), and optical properties (especially the SERS activity); these properties result from the high saturation magnetization of FePt NPs and the extinction coefficient and SERS activity of Ag NPs, which are the highest of any of the plasmonic NPs. By combining these two materials into single nanostructures (FePt@Ag NPs), high-performance dual-functional NPs can be obtained. To the best of our knowledge, there have been only a few successful examples of the synthesis of well-defined FePt@Ag core–shell NPs. Lu et al. synthesized well-defined FePt@Ag NPs using a two-stage reduction process with a seed-mediated technique [9]. However, the main objective of their work was to lower the temperature required for the phase transition from low magnetocrystalline anisotropy ( $K_u$ ) fcc-phase FePt to high  $K_u$  fct-phase FePt, which has the potential to be used as a high-density magnetic storage material, taking advantage of the Ag-doping effect during annealing. Therefore, the SERS activity and magnetic separation capabilities of FePt@Ag NPs have not yet been clarified. In addition, the mean size of the FePt@Ag NPs synthesized by Lu et al. was less than 10 nm, which is too small for most biological applications. For plasmonic imaging and SERS sensing applications, it is better if the volume of the Ag shell is larger than that of an Ag NP with a diameter of 10 nm. In addition, for magnetic separation, the bigger the FePt@Ag NPs are, the better, because it becomes more difficult to separate NPs as the NP size decreases. However, if the size exceeds ca. 50 nm, the colloidal stability of NPs is reduced, and cellular uptake decreases dramatically [10]. Roughly speaking, this means that there is an optimal size that lies somewhere between 10 and 50 nm, with the precise size depending on the intended purpose of the magnetic–plasmonic NPs.

In this work, we developed a scheme for the synthesis of well-defined FePt@Ag NPs with diameters larger than 10 nm, high SERS activity, high colloidal stability, and good magnetic separation capabilities, with the aim of using the NPs for biological sensing/imaging applications. The SERS activity of the FePt@Ag NPs was examined, using thiophenol as a Raman reporter molecule. In addition, the effects of the application of a magnetic field during the preparation of FePt@Ag NP films on the SERS activity were demonstrated.

## Experimental

### Chemicals

Platinum(II) acetylacetonate [Pt(acac)<sub>2</sub>; purity, 97 %], triiron dodecacarbonyl [Fe<sub>3</sub>(CO)<sub>12</sub>; purity, 99.999 %], silver

nitrate (AgNO<sub>3</sub>; purity, >99.0 %), tetraethylene glycol (TEG; purity, 99 %), oleic acid (OA; purity, 99 %), oleylamine (OLA; purity, 70 %), phenyl ether (purity, 99 %), and thiophenol (TP; purity, 97 %) were purchased from Sigma-Aldrich Corp.

### Synthesis of FePt Core NPs

First, superparamagnetic fcc-phase FePt NPs were synthesized using a previously reported method [11]. Uniform FePt NPs were formed at 240 °C under an Ar atmosphere by decomposing 85.37 mg (0.169 mmol) of Fe<sub>3</sub>(CO)<sub>12</sub> and reducing 100 mg (0.254 mmol) of Pt(acac)<sub>2</sub> in 20 mL of TEG, with the volume ratio of capping ligands OA/OLA = 1:1 fixing the total amount of ligands at OA+OLA = 9.3 mmol. After a reaction time of 2 h, the solution was left to cool to room temperature. The FePt NPs were purified and separated from the matrix by adding ethanol and centrifuging several times. The FePt NPs were then re-dispersed in hexane with OLA (5 vol%).

### Synthesis of FePt@Ag Core–Shell NPs

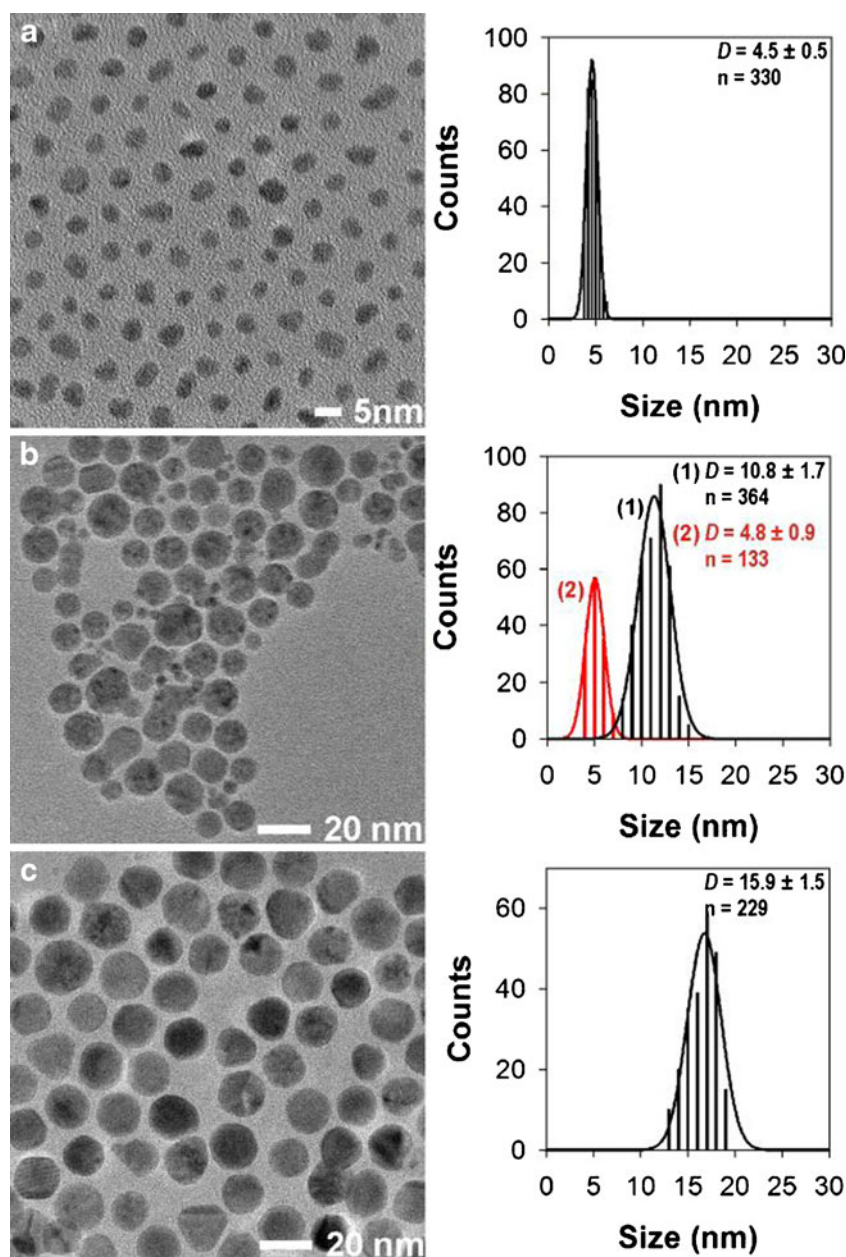
The as-synthesized OLA-capped FePt NPs were used as seeds to grow Ag shells. In a typical synthesis of FePt@Ag NPs with a Ag shell thickness of 5.7 nm, AgNO<sub>3</sub> (137.1 mg, 0.807 mmol) and OLA (2 mL, 6.09 mmol) were dissolved in 20 mL of phenyl ether and stirred for 30 min at 25 °C, under an Ar atmosphere. Then, 5 mL of the hexane dispersion of FePt NPs was injected into the solution. The reaction temperature was then raised to 80 °C, to completely remove the hexane from the reaction solution. Subsequently, the reaction temperature was raised to 200 °C; this temperature was maintained for 30 min. After the reaction, the reaction solution was left to cool to room temperature. The FePt@Ag NPs were then purified and separated from the matrix, by adding ethanol and centrifuging several times. The FePt@Ag NPs were re-dispersed in 30 mL of hexane, and the magnetically active NPs were then separated using a permanent magnet. This magnetic separation process was repeated three times. Finally, the purified FePt@Ag NPs were re-dispersed in hexane with OLA (5 vol%). The Ag shell thickness could be controlled by changing the amount of Ag precursor.

### Preparing Samples for SERS Measurements

Glass substrates were cleaned using sonication in acetone for 10 min, followed by another 10 min of sonication in methanol. Hexane dispersions of Ag, FePt, and FePt@Ag<sub>5.7</sub> (where the subscript denotes the Ag shell thickness in nanometer) NPs were prepared, keeping the NP concentration constant ( $3.6 \times 10^{-8}$  M). The SERS substrates were prepared

in two different ways. In the first method, 100  $\mu\text{L}$  of the NP dispersion was dropped onto the glass substrate and allowed to dry naturally (droplet deposition method, DD). In the other method, the glass substrate was dipped vertically into the NP dispersion, and the NPs accumulated on the surface of the glass substrate under the application of an external magnetic field (450 mT) for 4 h (magnetic deposition method, MD). The glass substrate was then removed from the NP dispersion and dried at room temperature, still under the magnetic field. We prepared four different SERS substrates: (1) Ag NP substrate prepared using DD (Ag\_DD), (2) FePt NP substrate prepared using MD (FePt\_MD), (3) FePt@Ag<sub>5.7</sub> substrate prepared using DD (FePt@Ag\_DD), and (4) FePt@Ag<sub>5.7</sub> substrate prepared using MD (FePt@Ag\_MD).

**Fig. 1** TEM images (*left*) and size distributions (*right*) of as-synthesized NPs: **a** FePt, **b** FePt@Ag<sub>3.2</sub>, and **c** FePt@Ag<sub>5.7</sub>



In the cases of Ag\_DD and FePt@Ag\_DD, relatively thick circular films with a diameter of approximately 1 cm were obtained. In the cases of FePt\_MD and FePt@Ag\_MD, however, relatively uniform large-area NP thin films were obtained. Then, a toluene solution of TP (100 nM) was dropped onto each SERS substrate and dried at room temperature. The TP molecules chemically adsorbed on the NP surfaces via metal–thiol interactions during the drying process.

#### Instrumentation and Measurements

The structure and composition of the as-synthesized NPs were fully characterized using transmission electron

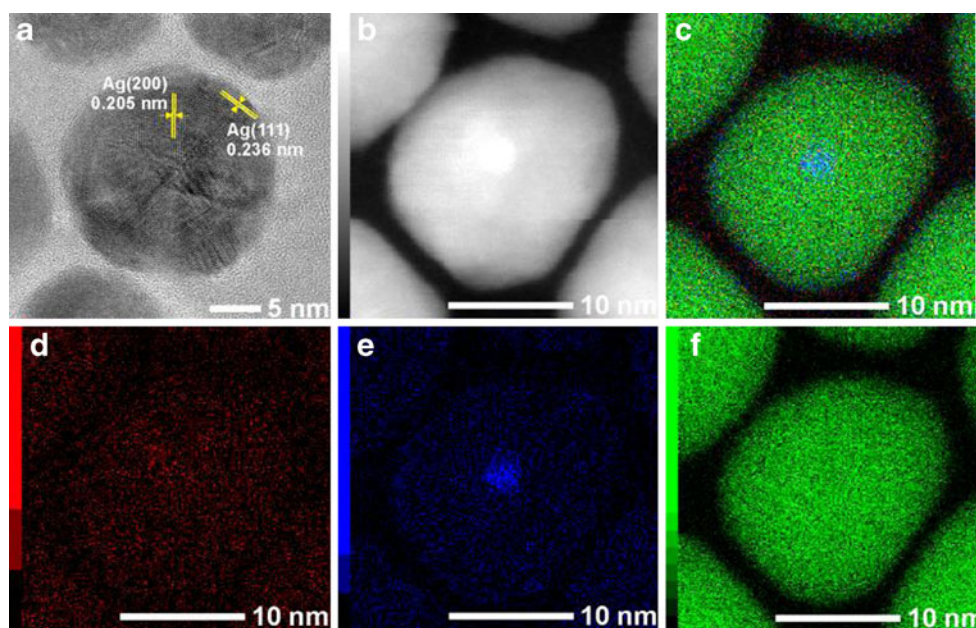
microscopy (TEM), high-resolution TEM (HRTEM), scanning TEM (STEM), energy-dispersive X-ray spectroscopy (EDS), and X-ray diffraction (XRD). TEM observations were performed on a Hitachi H-7100 operated at 100 kV. HRTEM was performed on a Hitachi H-9000NAR operated at 300 kV. EDS analysis was performed on a Hitachi H-7650 at 100 kV. STEM analysis and EDS elemental mapping were performed on a JEOL JEM-ARM200F instrument operated at 200 kV with a spherical aberration corrector; the nominal resolution was 0.8 Å. The crystal structures of NPs were identified using a Rigaku SmartLab X-ray diffractometer with Cu K $\alpha$  radiation ( $\lambda=1.542$  Å, 40 kV, 30 mA). Dynamic light scattering (DLS) measurements were carried out using a high-performance particle sizer (Malvern). The absorption spectra of the NP dispersions were collected using a PerkinElmer Lambda 35 UV–vis spectrometer. The magnetic properties of the NPs were measured on a SQUID magnetometer (Quantum Design, MPMS). The mass of surface capping ligands present in the samples was measured using thermogravimetry analysis (TGA). TGA was performed using a Seiko TG/DTA6200. Samples underwent heat treatment from 25 to 600 °C in flowing nitrogen gas, with a heating rate of 10 °C/min. SERS spectra were obtained with an Ar<sup>+</sup> ion laser (wavelength, 514.5 nm; power, 50 mW), using a Horiba-Jobin Yvon Ramanor T64000 triple monochromator equipped with a CCD detector. The nonpolarized Raman scattering measurements were performed under a microscope sample holder, using a 180° backscattering geometry, at room temperature. The laser spot diameter was 1  $\mu$ m. The acquisition time was 30 s per spectrum, so for each measurement, we averaged three spectra taken from the same area.

## Results and Discussion

The as-synthesized FePt NPs were quite uniform in size and shape, as shown in Fig. 1a. The FePt NPs had an average diameter of  $4.5\pm 0.5$  nm. According to the EDS results, the composition of the FePt NPs was Fe<sub>46</sub>Pt<sub>54</sub>. Panels b and c of Fig. 1 show TEM images of the FePt@Ag<sub>3,2</sub> and FePt@Ag<sub>5,7</sub> NPs, respectively. In the case of FePt@Ag<sub>3,2</sub> NPs, small NPs of diameter of  $4.8\pm 0.9$  nm were observed, along with larger NPs with a diameter of  $10.8\pm 1.7$  nm (Fig. 1b). These small NPs were uncoated FePt NPs and/or FePt NPs coated with a very thin Ag shell. The possibility of the existence of small Ag NPs can be ruled out, because the NPs were magnetically separated. In the case of FePt@Ag<sub>5,7</sub> NPs (mean diameter,  $15.9\pm 1.5$  nm), on the other hand, the size distribution was unimodal, with no small NPs (Fig. 1c).

These results can be understood using the La Mer model [12]. During the seed-mediated growth reaction of the Ag shell, the Ag atoms/clusters are deposited on the FePt cores; once this occurs, they act as active sites for further Ag deposition, allowing the formation of continuous Ag shells via the creation of Ag nanocrystals. However, when the relative concentration of the Ag precursor is not high enough, the Ostwald ripening effect becomes more dominant and begins to compete with the deposition reaction. Therefore, Ag nanocrystals larger than the critical size will grow at the expense of crystals smaller than the critical size in the ripening regime. For FePt@Ag<sub>3,2</sub> NPs, this leads to a bimodal size distribution of NPs that consists of FePt@Ag NPs with a thick Ag shell and FePt NPs with no coating or only a very thin coating of Ag. In the case of FePt@Ag<sub>5,7</sub> NPs, however, the Ag precursor concentration was high

**Fig. 2** a HRTEM, b HAADF-STEM, and c–f EDS elemental mapping images of an individual FePt@Ag<sub>5,7</sub> NP: c overlay, d Fe K edge, e Pt M edge, and f Ag L edge



enough to suppress the ripening, and the Ag shells therefore grew uniformly.

To confirm the core–shell structure, HRTEM and STEM analyses were performed on an individual FePt@Ag<sub>5.7</sub> NP. Figure 2a shows an HRTEM image of an individual FePt@Ag<sub>5.7</sub> NP. Lattice fringes with *d*-spacing values of 0.236 and 0.205 nm—which respectively corresponded to the (111) and (200) planes of fcc-phase Ag (JCPDS card no. 01-071-3762)—were clearly identified. Figure 2b shows a high-angle annular dark-field (HAADF) STEM image of an individual FePt@Ag<sub>5.7</sub> NP. A bright spherical center and a less bright shell can be clearly observed, indicating that heavy Pt atoms were in the core, and light Ag atoms were in the shell. Panels c–f of Fig. 2 show two-dimensional EDS elemental mapping images of an FePt@Ag<sub>5.7</sub> NP. It was clear that Pt was found in the core area, and Ag was found in the shell area. The spatial resolution of EDS mapping is primarily governed by the degree of penetration and scattering of the electron beam in the specimen, which may be highly influenced by the relative size of the materials imaged and the fact that the NPs are three dimensional in nature, while the resulting composition map is two dimensional (resulting in less resolution at the NP edges). Because of these limitations in the spatial resolution for the elemental mapping technique, the FePt core appears smaller than its actual size (4.5±0.5 nm). In addition, small amounts of Fe and Pt are observed in the shell area, presumably due to background signal accumulation caused by the long measurement time (90 min). The EDS elemental mapping experiment was also used to confirm the oxidation properties of the Ag shell in both Ag and FePt@Ag NPs. No significant level of oxidation was observed for these samples, which is expected based on the ability of OLA to protect

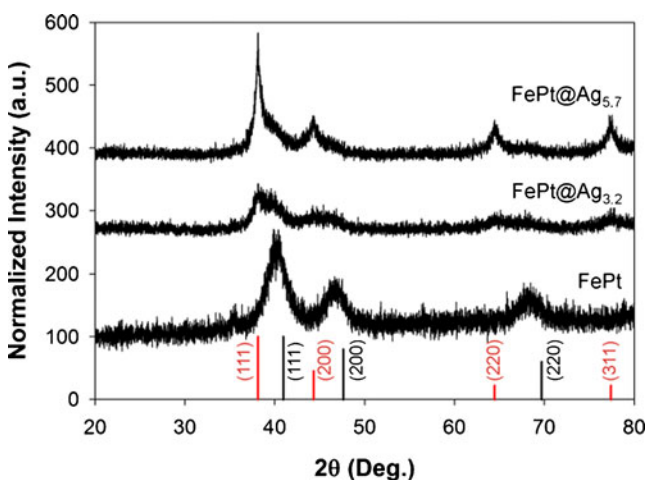


**Fig. 3** XRD patterns for as-synthesized NPs: FePt (bottom), FePt@Ag<sub>3.2</sub> (middle), and FePt@Ag<sub>5.7</sub> (top) NPs. The reference peaks are for fcc FePt (black, JCPDS card no. 00-029-0718) and fcc Ag (red, JCPDS card no. 01-071-3762)

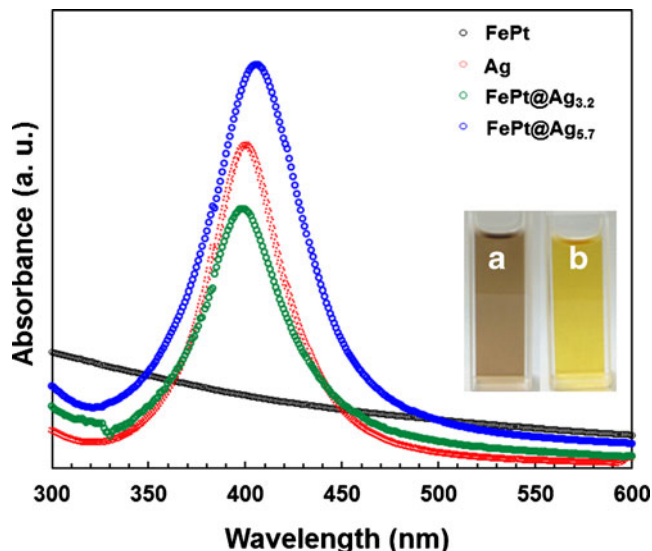


**Fig. 4** UV–vis spectra for FePt (black), Ag (red), FePt@Ag<sub>3.2</sub> (green), and FePt@Ag<sub>5.7</sub> (blue). The inset shows a photograph of the diluted suspensions of FePt (A) and FePt@Ag<sub>5.7</sub> (B) NPs

the surface of these NPs against oxidation. Figure 3 shows the XRD patterns for FePt, FePt@Ag<sub>3.2</sub>, and FePt@Ag<sub>5.7</sub> NPs. The FePt NPs showed a chemically disordered fcc phase, and the Ag shells showed an fcc phase. The mean crystalline size of the FePt NPs was calculated to be 3.9 nm, using the Scherrer formula. When the Ag shell thickness was increased, the Ag peaks became more intense and narrower, indicating that the crystalline size increased. These results definitively showed that well-defined FePt@Ag core–shell NPs were successfully synthesized.

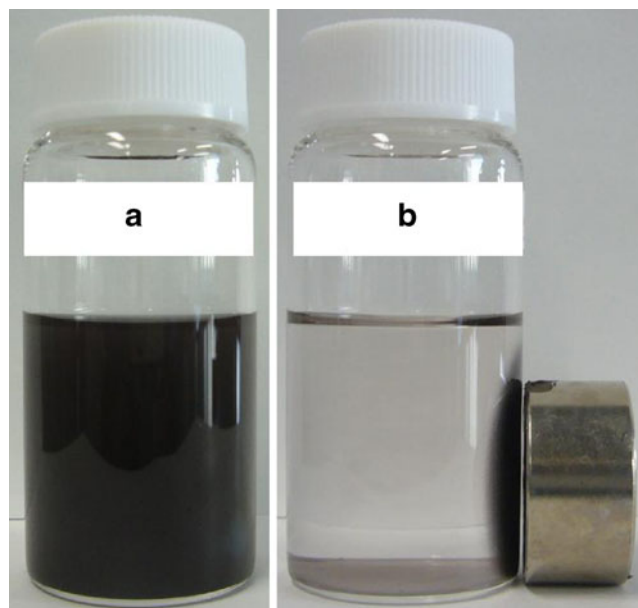


**Fig. 5** Photographs of FePt@Ag<sub>5.7</sub> NPs in hexane without (a) and with magnet (b)

Figure 4 shows the UV–vis absorption spectra for Ag, FePt, and FePt@Ag<sub>3,2</sub>. Note that the Ag NPs were synthesized under the same reaction conditions as those used for the FePt@Ag<sub>5,7</sub> NPs in the absence of FePt seeds. The mean size of the Ag NPs was  $15.8 \pm 3.0$  nm (Supporting Information, Fig. S1). For UV–vis analysis, the NP dispersions were diluted by a factor of 18 to achieve adsorption spectra with a reasonable intensity. The Ag and FePt@Ag NPs exhibited a LSPR peak in the visible region, while the FePt NPs showed only a broad absorption profile. The LSPR peak wavelengths for Ag, FePt@Ag<sub>3,2</sub>, and FePt@Ag<sub>5,7</sub> NPs were 399, 397, and 412 nm, respectively. It is noteworthy that the LSPR peak for the FePt@Ag<sub>5,7</sub> NPs was slightly redshifted compared with that for the Ag NPs. The same trend has been reported for FePt@Ag core–shell NPs [9] and can be attributed to the core–shell nanostructure (Ag nanoshell structure) [9, 13].

The colloidal stability of the FePt@Ag NPs was evaluated by measuring the size distribution of the NPs in hexane,

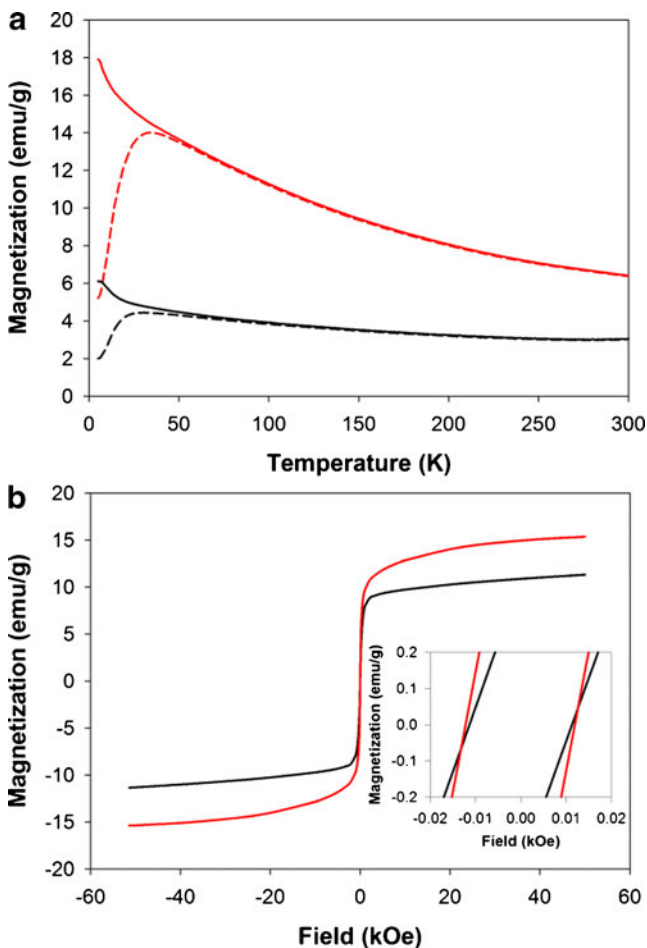


**Fig. 6** **a** FC (solid lines) and ZFC (dashed lines) magnetization versus temperature curves for the FePt (black) and FePt@Ag<sub>5,7</sub> (red) NPs. **b** Magnetization versus applied field curves for FePt (black) and FePt@Ag<sub>5,7</sub> (red) NPs, measured at 300 K. The inset shows a magnified view of the hysteresis loops at low magnetic field

using DLS. The FePt@Ag<sub>5,7</sub> NP dispersion was stored under ambient laboratory conditions for 2.5 months, and the hydrodynamic diameter of the NPs in the dispersion was then measured. The average size was found to be 21.5 nm (Supporting Information, Fig. S2), with no signs of aggregation; this indicated that the FePt@Ag NPs were quite stable. The FePt@Ag NPs could be easily collected using a magnet, as shown in Fig. 5. The FePt@Ag NPs can therefore be regarded as excellent potential magnetic–plasmonic dual-functional probes for various biological applications in which both manipulation and monitoring are required.

Figure 6a shows the temperature dependence of magnetization (zero-field cooling (ZFC) and field cooling (FC) curves) for the as-synthesized FePt and FePt@Ag<sub>5,7</sub> NPs, measured in a magnetic field of 500 Oe. The values of magnetization for the NPs were normalized using the weight of the magnetic FePt core. Note that the mass fraction of surface capping ligands present in the sample was determined using TGA (Supporting Information, Fig. S3). In the case of the FePt NPs, the mass fraction of capping ligands was 7 %, and it was 5 % for the FePt@Ag<sub>5,7</sub> NPs. The blocking temperature  $T_B$  was determined from the merge point of the ZFC and FC curves, and was found to be approximately 52 K for both samples; the magnetocrystalline anisotropy constant ( $K_u$ ) was calculated to be  $376 \text{ kJ/m}^3$  for both the FePt and FePt@Ag<sub>5,7</sub> NPs, using the following equation:  $K_u = 25k_B T_B / V$ , where  $k_B$  and  $V$  are the Boltzmann constant and the volume of a FePt magnetic core, respectively. This value of  $K_u$  was consistent with the  $K_u$  value for fcc FePt NPs [14].

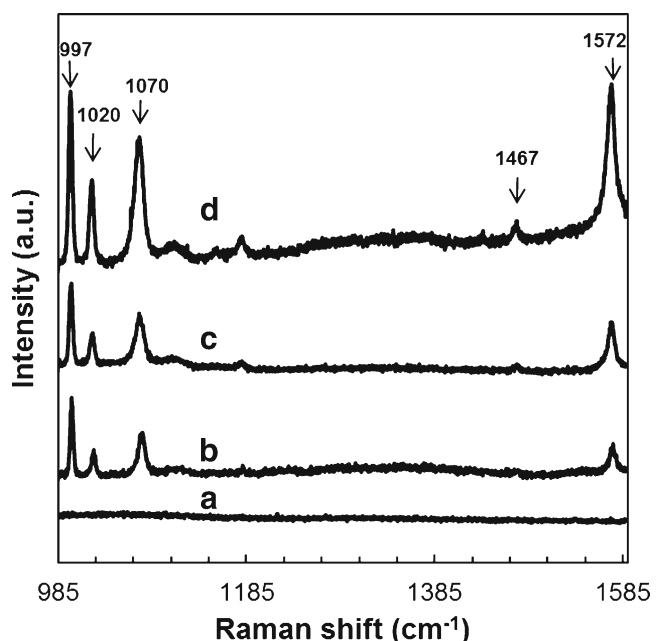


**Fig. 7** SERS spectra of TP obtained using *A* FePt\_MD, *B* Ag\_DD, *C* FePt@Ag\_DD, and *D* FePt@Ag\_MD

Figure 6b shows the magnetization curves measured as a function of the applied field at 300 K. Both NPs clearly showed superparamagnetic behavior. The saturation magnetization ( $M_s$ ) was estimated to be 11 emu/g for the FePt NPs, while the  $M_s$  for the FePt@Ag<sub>5.7</sub> NPs was 15 emu/g. The  $M_s$  of the FePt@Ag<sub>5.7</sub> NPs was found to be higher than that of FePt NPs, suggesting that the Ag shell effectively passivated the FePt NP surfaces, avoiding the direct interaction between the FePt core and surface capping ligands that typically forms a magnetically dead layer in FePt NPs [15, 16]. To estimate the thickness of the dead layer for each NP, we considered the FePt NPs as a magnetic core coated with the dead layer of thickness of  $\delta$ . The volume magnetization for FePt and FePt@Ag<sub>5.7</sub> was 154 and 210 emu/cm<sup>3</sup>, respectively. It is assumed that the dead layer has zero magnetization, and the magnetic core shows full magnetization, i.e., the theoretical value for FePt NPs (600 emu/cm<sup>3</sup>) [17]. As a result,  $\delta$  was estimated to be 0.82 and 0.66 nm for FePt and FePt@Ag NPs, respectively. Those values are thought to be quite reasonable when compared to the lattice constant of fcc FePt (0.38 nm). The hysteresis observed in Fig. 6b arises from a small fraction of NPs that exhibit the more magnetically anisotropic fct phase of FePt, which originates in the relatively high temperature (240 °C) and long time (2 h) synthesis of the core particles [9].

Finally, the SERS activity of the FePt@Ag<sub>5.7</sub> NPs was investigated, using TP as a Raman reporter molecule. Figure 7 shows the Raman spectra of TP obtained using FePt\_MD, Ag\_DD, FePt@Ag\_DD, and FePt@Ag\_MD. In the case of FePt\_MD, no peak was observed, reflecting the SERS-inert nature of FePt NPs. In the case of Ag\_DD, on the other hand, four distinct peaks were observed at 997, 1,020, 1,070, and 1,572 cm<sup>-1</sup>. These peaks corresponded to S–H bending, in-plane ring deformation, C–S stretching, and C–C stretching vibrations, respectively [18, 19]. FePt@Ag\_DD yielded a similar SERS spectrum to Ag\_DD, indicating that the FePt@Ag<sub>5.7</sub> NPs had almost the same SERS activity as Ag NPs. Interestingly, however, FePt@Ag\_MD showed an enhanced SERS activity compared with FePt@Ag\_DD; some other weak peaks appeared at 1,110, 1,180, and 1,467 cm<sup>-1</sup>. The first two peaks could not be assigned, but the peak at 1,467 cm<sup>-1</sup> corresponded to the Ag–S vibration [18]. The explanation for the enhanced SERS signal of FePt@Ag\_MD can be given as follows: FePt@Ag\_MD does not contain any nonmagnetic species such as free OLA (excess) molecules that can hinder the adsorption of TP molecules on the FePt@Ag NP surfaces. In addition, as a result of the magnetic dipole–dipole interaction, FePt@Ag NPs can rearrange during drying to become more closely packed in the film, thus increasing the number density of hot spots and/or changing the interparticle separation distance to favor an increase in the SERS activity. The Raman results are internally consistent given the fact that Ag and FePt@Ag<sub>5.7</sub> NPs are virtually

identical in size, and the deposition techniques ensure NP layers that are much thicker than the optimum Raman beam penetration depth (ensuring identical analysis volumes of each sample). These results clearly demonstrated the great potential of magnetic–plasmonic FePt@Ag core–shell NPs for biological sensing/imaging applications; they show high colloidal stability, good magnetic separation capabilities, and enhanced SERS activity. In addition, one can easily make thin films on solid substrates in the position where they are needed. Although these NPs must be made water soluble for real-world bio-applications, a wide variety of ligand-exchange techniques can be applied to achieve this goal. For example, we have already developed a ligand-exchange protocol to make hydrophobic FePt NPs water soluble using 2-aminoethanethiol molecules and have succeeded in obtaining NH<sub>2</sub>-terminated water-dispersible FePt NPs [20]. This technique is definitely also applicable for FePt@Ag core–shell NPs, and studies are currently underway to investigate this.

In summary, a new synthetic route was developed for the fabrication of well-defined FePt@Ag NPs with a diameter of 16 nm that exhibit both superparamagnetic and plasmonic properties. The magnetic–plasmonic FePt@Ag NPs show high colloidal stability, good magnetic separation capabilities, and enhanced SERS activity. These FePt@Ag NPs show great promise as probes for various biomedical applications, including plasmonic bioimaging, magnetic cell separation, and magnetic immuno assays.

**Acknowledgments** The authors thank Dr. Mikio Koyano and Ms. Dao T. Ngoc Anh for their assistance with the Raman measurements. NTTT thanks the Vietnamese Government for a 322 scholarship.

## References

1. Sotiriou GA, Hirt AM, Lozach PY, Teleki A, Krumeich F, Pratsinis SE (2011) Hybrid, silica-coated, janus-like plasmonic-magnetic nanoparticles. *Chem Mater* 23:1985–1992
2. Smolensky ED, Neary MC, Zhou Y, Berquo TS, Pierre VC (2011) Fe<sub>3</sub>O<sub>4</sub>@organic@Au: core-shell nanocomposites with high saturation magnetization as magnetoplasmonic MRI contrast agents. *Chem Commun* 47:2149–2151
3. Gao J, Zhang B, Gao Y, Pan Y, Zhang X, Xu B (2007) Fluorescent magnetic nanocrystals by sequential addition of reagents in a one-pot reaction: a simple preparation for multifunctional nanostructures. *J Am Chem Soc* 129:11928–11935
4. He S, Zhang H, Delikanli S, Qin Y, Swihart MT, Zeng A (2009) Bifunctional magneto-optical FePt-CdS hybrid nanoparticles. *J Phys Chem C* 113:87–90
5. Lin HY, Chen YF, Wu JG, Wang DI, Chen CC (2006) Carrier transfer induced photoluminescence change in metal–semiconductor core-shell nanostructures. *Appl Phys Lett* 88:161911–161913
6. Jiang J, Gu H, Shao H, Devlin E, Papaefthymiou GC, Ying JY (2008) Bifunctional Fe<sub>3</sub>O<sub>4</sub>-Ag heterodimer nanoparticles for two-photon fluorescence imaging and magnetic manipulation. *Adv Mater* 20:4403–4407

7. Levin CS, Hofmann C, Ali TA, Kelly AT, Morosan E, Nordlander P, Whitmire KH, Halas NJ (2009) Magnetic-plasmonic core-shell nanoparticles. *ACS Nano* 3:1379–1388
8. de la Presa P, Multigner M, Morales MP, Rueda T, Fernández-Pinel E, Hernando A (2007) Synthesis and characterization of FePt/Au core-shell nanoparticles. *J Magn Magn Mater* 316:e753–e755
9. Lu LY, Wang D, Xu XG, Wang HC, Miao J, Jiang Y (2011) Low temperature magnetic hardening in self-assembled FePt/Ag core-shell nanoparticles. *Mater Chem Phys* 129:995–999
10. Chithrani BD, Ghazani AA, Chan WCW (2006) Determining the size and shape dependence of gold nanoparticle uptake into mammalian cells. *Nano Lett* 6:662–668
11. Trinh TT, Mott D, Thanh NTK, Maenosono S (2011) One-pot synthesis and characterization of well defined core-shell structure of FePt@CdSe nanoparticles. *RSC Adv* 1:100–108
12. La Mer VK, Dinegar RH (1950) Theory, production and mechanism of formation of monodispersed hydrosols. *J Am Chem Soc* 72:4847–4854
13. Prodan E, Radloff C, Halas NJ, Nordlander PA (2003) A hybridization model for the plasmon response of complex nanostructures. *Science* 302:419–422
14. Maenosono S, Saita S (2006) Theoretical assessment of FePt nanoparticles as heating elements for magnetic hyperthermia. *IEEE Trans Magn* 42:1638–1642
15. Wu XW, Liu C, Li L, Jones P, Chantrell RW, Weller D (2004) Nonmagnetic shell in surfactant-coated FePt nanoparticles. *J Appl Phys* 95:6810–6812
16. Trinh TT, Ozaki T, Maenosono S (2011) Influence of surface ligands on magnetic property of FePt clusters: a density functional theory calculation. *Phys Rev B* 83:104413
17. Taylor RM, Huber DL, Monson TC, Esch V, Sillerud LO (2012) Structural and magnetic characterization of superparamagnetic iron platinum nanoparticle contrast agents for magnetic resonance imaging. *J Vac Sci Technol B* 30:02C101–02C107
18. Jung HY, Park YK, Park S, Kim SK (2007) Surface enhanced Raman scattering from layered assemblies of close-packed gold nanoparticles. *Anal Chim Acta* 602:236–243
19. Li X, Cao M, Zhang H, Zhou L, Cheng S, Yao JL, Fan LJ (2012) Surface-enhanced Raman scattering-active substrates of electrospun polyvinyl alcohol/gold-silver nanofibers. *J Colloid Interface Sci* 382:28–35
20. Tanaka Y, Maenosono S (2008) Amine-terminated water-dispersible FePt nanoparticles. *J Magn Magn Mater* 320:L121–L124